Constructing Quantum Dots@Flake g-C_3N_4 Isotype Heterojunctions for Enhanced Visible-Light-Driven NADH Regeneration and Enzymatic Hydrogenation

Dong Yang[a,c], Hongjian Zou[a], Yizhou Wu[a], Jiafu Shi[b,c,], Shaohua Zhang[a], Xiaodong Wang[e], Pingping Han[a], Zhenwei Tong[a], Zhongyi Jiang[a,b,d*]*

[a]Key Laboratory for Green Chemical Technology of Ministry of Education, School of Chemical Engineering and Technology, Tianjin University, Tianjin 300072, China;

[b]State Key Laboratory of Biochemical Engineering, Institute of Process Engineering, Chinese Academy of Sciences, Beijing, 10090, China;

[c]School of Environmental Science and Engineering, Tianjin University, Tianjin 300072, China;

[d]Collaborative Innovation Center of Chemical Science and Engineering (Tianjin), Tianjin 300072, China;

[e]School of Engineering, University of Aberdeen, Aberdeen AB24 3UE, Scotland, UK

* Corresponding author: Jiafu Shi, shijiafu@tju.edu.cn; Zhongyi Jiang, zhyjiang@tju.edu.cn

KEYWORDS: NADH regeneration, enzymatic hydrogenation, isotype heterojunctions, quantum dots, flake g-C_3N_4

ABSTRACT

NAD(P)H is a critical cofactor (biological source of hydrogen) that participates in many enzymatic hydrogenations for energy conversion and storage with resultant oxidation to $NAD(P)^+$. Due to its high cost, the regeneration of NAD(P)H is a critical and feasible way to ensure the sustainability of these enzymatic hydrogenations. Intrigued by the photoreaction process in thylakoid membrane, we explored a two-dimensional (2D) isotype heterojunction photocatalyst, termed as quantum dots@flake graphitic carbon nitride (QDs@Flake g-C_3N_4), for visible-light-driven NAD(P)H regeneration. The catalyst was synthesized by one-step calcination using cyanamide-treated cyanuric acid-melamine (CM) complex as starting material, where cyanamide plays dual roles: a) assisting the transformation of CM from bulky to stacked structure and further to flakes after calcination, and b) acting as raw material for the generation of QDs on the flakes. To replicate both the functional and structural properties of the natural photoreaction system, QDs@Flake g-C_3N_4 exploited the two types of g-C_3N_4 (*i.e.*, QDs and flake) and a heterojunction interface to, respectively, mimic the functional components of light-harvesting systems (LHSs, *i.e.*, PS I and PS II) and electron transport chains (ETCs), and utilized the flake structure as the analogue of 2D thylakoid membrane. Therefore, QDs@Flake g-C_3N_4 showed remarkably improved capability in visible light harvesting and charge separation, and exhibited elevated performance in photocatalytic NADH regeneration with a regeneration yield of up to 40%. The NADH regeneration approach was then coupled with alcohol dehydrogenase-catalyzed hydrogenation of formaldehyde, achieving

continuous methanol production.

1. INTRODUCTION

Enzymatic hydrogenation refers to the catalyzed reduction of molecules with higher-valence carbon (carbon dioxide (CO_2), formate, formaldehyde, *etc.*) by oxidoreductases that are a kind of enzyme accounting for 30% of commercial enzymes. Enzymatic hydrogenation has been extensively applied and displayed high performance for energy conversion and storage, such as CO_2 fixation and alcohol synthesis, due to the mild reaction conditions, exceptional activity and regio-/stereo-selectivity, [1, 2] *etc*. Such hydrogenation processes rely on the sustainable supply of hydrides in the form of NAD(P)H as nearly 90% of known oxidoreductases require NAD(P)H as a cofactor. The stoichiometric addition of high-cost NAD(P)H (>$100 per gram) is too expensive for industrialization of enzymatic hydrogenation, [3, 4] and thus the effective NAD(P)H regeneration strategies are eagerly expected. [5-7]

Solar energy, as a kind of green and sustainable energy sources, has received lots of interests. In nature, green plants, algae and cyanobacteria are experts to convert and store solar energy in the form of chemicals, such as NAD(P)H, through photoreaction process. Such a process basically relies on several key functional components (chlorophyll, phycobilisome, plastoquinone, cytochrome *b6f*, plastocyanin, *etc*.) and unique structure (two-dimensional (2D) thylakoid membrane). [8-10] The key functional components comprise light-harvesting systems (LHSs) and electron transfer chains (ETCs), which are critical in the natural photoreaction system. Specifically, LHSs that include photosystem I (PS I) and photosystem II (PS II) are composed of some

light-harvesting antenna (*e.g.*, chlorophyll, phycobilisome). The co-initiation of PS I and PS II by visible light ensures the high efficiencies in the utilization of visible light and photo-excitation of electrons. ETCs that comprise plastoquinone, cytochrome *b6f* and plastocyanin could facilitate the transfer of the photo-excited electrons to ferredoxins for further NAD(P)H regeneration. Interestingly, LHSs and ETCs are both located within/on the 2D thylakoid membrane, which ensures the photo-excitation and electron transfer processes to occur in a confined space and, particularly, enables photo-excited electrons transferred in an oriented manner. [11] Inspired by the photoreaction process in thylakoid membrane, constructing 2D artificial photocatalytic systems with visible-light harvesting and oriented electron transfer capabilities would be an efficient method for NADH regeneration. It should be noted that, although several research groups have developed a series of photocatalytic systems for NADH regeneration, no reports is related to 2D structured photocatalysts. [12-16]

Recently, isotype heterojunction semiconductors have drawn broad interests in various disciplines owing to their unique electronic band structure. It is well recognized that isotype heterojunctions could promote the dissociation of electron-hole pairs through co-initiating the two moieties of the heterojunction by light, facilitate the collection and transfer of charge at the heterojunction interface, and finally minimize the charge recombination. [17-21] In this regards, isotype heterojunction semiconductors have some similarities to LHSs and ETCs in the natural photoreaction system. Given the visible-light harvesting capability and the

designable property of electronic band structure, carbon nitride (CN) exhibits versatility and superiority in constructing isotype heterojunctions. [22] Typically, Wang and co-workers [20] prepared bulky CN/CNS isotype heterojunctions through two-step calcination by using dicyandiamide and trithiocyanuric acid as CN and sulfur(S)-containing CN precursors, respectively. Such bulky CN/CNS isotype heterojunctions exhibited higher charge separation efficiency, and enhanced photocatalytic activity of 11 times higher than that of bulky CN for hydrogen evolution. Since then, several kinds of CN-based bulky isotype heterojunctions were designed and synthesized using similar procedure. [17-19] Albeit some achievements, the structures of CN-based isotype heterojunctions were mostly in bulky type, which were rarely engineered into 2D sheets/flakes such like 2D thylakoid membrane. Recent reports indicated that 2D graphitic carbon nitrite (g-C_3N_4) sheets/flakes showed much higher efficiency of photo-excited charge transfer and separation. For instance, Tong *et al.* [23] and Zhang *et al.* [24] synthesized ultrathin g-C_3N_4 sheets by the liquid exfoliation route from bulky g-C_3N_4, which could promote the charge migration and separation efficiency by two more times in comparison to bulky g-C_3N_4. Therefore, CN-based 2D isotype heterojunctions would integrate the merits of 2D sheets/flakes structure and CN-based heterojunctions, which would benefit to elevating the photocatalytic efficiency during the NADH regeneration.

In this study, for the first time, a 2D isotype heterojunction photocatalyst, termed as quantum dots@flake g-C_3N_4 (QDs@Flake g-C_3N_4), was reported for visible-light-driven NADH regeneration. The construction of QDs@Flake g-C_3N_4

aims to replicate both the functional and structural properties of the natural photoreaction system. The two types of g-C_3N_4 (*i.e.*, QDs and flake) and a heterojunction interface were, respectively, employed to mimic the functional components of LHSs (*i.e.*, PS I and PS II) and ETCs, whereas the flake structure was designed as the analogue of 2D thylakoid membrane. Compared to bulky g-C_3N_4, the resultant QDs@Flake g-C_3N_4 showed relatively large specific surface area and high separation/migration rate of photo-generated electrons-hole pairs, thus leading to enhanced NADH regeneration efficiency. Furthermore, the photocatalytic NADH regeneration was coupled with enzymatic hydrogenation of formaldehyde to methanol catalyzed by yeast alcohol dehydrogenase (YADH), which could continuously offer hydrides for formaldehyde, demonstrating the potential of our photocatalysts in energy conversion and storage.

2. EXPERIMENTAL

2.1 Materials:

Melamine (99%) and cyanuric acid (98%) were purchased from Guangfu Chemical Reagent Tianjin Co., Ltd. (Tianjin, China). Cyanamide (50 w/w%), triethanolamine (TEOA) was obtained from Aladdin Industrial Corporation (Shanghai, China). Rhodium (III) chloride hydrate, 2, 2'-bipyridyl, 1, 2, 3, 4, 5-pentamethylcyclopentadiene, β-nicotinamide adenine dinucleotide phosphate sodium salt hydrate (β-NAD^+), disodium hydrogen phosphate and sodium dihydrogen phosphate were received from Sigma-Aldrich (St. Louis, USA). All other chemicals

were of analytical grade and used without further treatment.

2.2 Preparation of quantum dots (QDs)@Flake g-C_3N_4 isotype heterojunctions:

In a typical procedure, 70 mL equal molar ratio of cyanuric acid and melamine (0.024 M) were mixed under magnetic stirring at 42 ^oC. [25] Then, the obtained white precipitates were collected by centrifugation at a speed of 6000 rpm for 1 minute (denoted as CM), which were then mixed with 50 w/w% cyanamide followed by oscillation for 30 minutes and vacuum drying at 40 ^oC. The complex was placed in a porcelain crucible with a cover and heated at 4.5 $^oC\ min^{-1}$ up to 550 ^oC in air for 4 h. The resultant sample was labeled as QDs@Flake g-C_3N_4.

2.3 Preparation of g-C_3N_4-CM:

Briefly, 70 mL equal molar ratios of cyanuric acid and melamine were mixed under magnetic stirring at 42 ^oC. Then, the obtained white supramolecular CM was collected by centrifugation at the rate of 6000 rpm for 1 min. After removal of surplus water under vacuum drying at 40 ^oC, the white solid (CM) was placed in a porcelain crucible with a cover and heated at 4.5 $^oC\ min^{-1}$ up to 550 ^oC for 4 h in air. The resultant yellow powder was denoted as g-C_3N_4-CM.

2.4 Preparation of g-C_3N_4-Cya:

Bulky g-C_3N_4 was directly synthesized by thermal polycondensation of crystal cyanamide from room temperature to 550 ^oC in air with a ramp rate of 4.5 $^oC\ min^{-1}$ and held for 4 h, then cooled to room temperature. The resultant product was denoted as g-C_3N_4-Cya.

2.5 Preparation of $[Cp^*Rh(bpy)H_2O]^{2+}$:

$RhCl_3 \cdot H_2O$ was refluxed in methanol with one equivalent of 1, 2, 3, 4, 5-pentamethylcyclopentadiene for 24 h. The resultant red precipitate was filtrated and suspended in methanol. After the addition of two equivalents of 2, 2-bipyridine, the suspension was cleared up and a yellowish solution was acquired. [Cp*Rh(bpy)Cl]Cl was precipitated through adding diethyl ether into the yellowish solution. A stock solution (100 mM) of [Cp*Rh(bpy)Cl]Cl was prepared in water and stored at room temperature without direct light exposure. Note that [Cp*Rh(bpy)Cl]Cl could readily hydrolyze to $[Cp^*Rh(bpy)(H_2O)]^{2+}$ in aqueous solution. [26]

2.6 Photocatalytic regeneration of NADH:

In a typical regeneration procedure, the reaction system was composed of β-NAD^+, TEOA (10.0 w/v%), phosphate buffer (100 mM, pH = 9.0) and photocatalyst (1 mg mL^{-1}) at 25 ^oC. The suspension (20 mL) was placed into a quartz reactor equipped with a stirring bar and illuminated with a 500 W Xe lamp (Beijing AuLight Technology Co.) with a cutoff filter ($\lambda \geq 420$ nm). The distance between 500 W Xe lamp and the reactor was fixed at 10 cm. Before illumination, the reaction solution was placed in dark for 1 h to accomplish the adsorption–desorption equilibrium. During the illumination, the NADH concentration was calculated by measuring the absorbance of the solution at 340 nm with a UV-vis spectrophotometer (U-3010, Hitachi).

2.7 Enzymatic hydrogenation of formaldehyde with in situ NADH regeneration:

The reaction medium for coupling NADH regeneration with enzymatic (yeast alcohol dehydrogenase, YADH) hydrogenation includes β-NAD^+ or NADH (20 mM), formaldehyde (30 mM), YADH (1.0 mg mL^{-1} stock solution: 10 mg YADH was dissolved in 10 mL phosphate buffer (100 mM, pH = 9.0)), TEOA (10.0 w/v%), different photocatalysts (1 mg mL^{-1}) and 100 mM phosphate buffer at pH = 9.0 at 25 °C. The volume of the reaction solution was 20 mL. Before the illumination, the reaction solution was placed in a dark environment for 60 minutes to accomplish the adsorption–desorption equilibrium. During the illumination, the methanol conversion yield was recorded for given time intervals by gas chromatography (Agilent GC 7820B).

2.8 Characterizations:

Scanning electron microscope (SEM) was carried out on an FEI Nova XL430 and Hitachi Limited instrument. TEM images were taken on FEI Tecnai G2 F20 equipment. Powder X-ray diffraction (XRD) measurements were performed on a Rigaku D/max 2500V/PC X-ray diffractometer (Cu Kα, λ = 0.154 nm, 40 kV, 200 mA), and the data was acquired in the range of 5- 60 ^{o} (2θ) at a rate of 4 ^{o} min^{-1}. Fourier transform infrared spectroscopy (FT-IR) was measured on a Nicolet-560 spectrometer, where 32 scans were accumulated with a resolution of 4 cm^{-1} for each spectrum. The X-ray photoelectron spectroscopy (XPS) was performed on a Perkin- lmer PHI 1600 ESCA X-ray photoelectron spectroscope with monochromatic Mg Kα radiation (1253.6 eV). Nitrogen adsorption-desorption isotherms were done with a TRISTAR-3000 surface area analyzer at 77 K. The UV-vis absorption spectra

were recorded by a UV-vis spectrophotometer (U-3010, Hitachi) equipped with an integrating sphere for the diffuse-reflectance spectroscopy (DRS), using $BaSO_4$ as reference. Photoluminescence spectra were recorded on Jobin Yvon Fluorolog 3-21 fluorescence spectrometer at room temperature with excitation at 375 nm.

3. RESULTS AND DISCUSSION

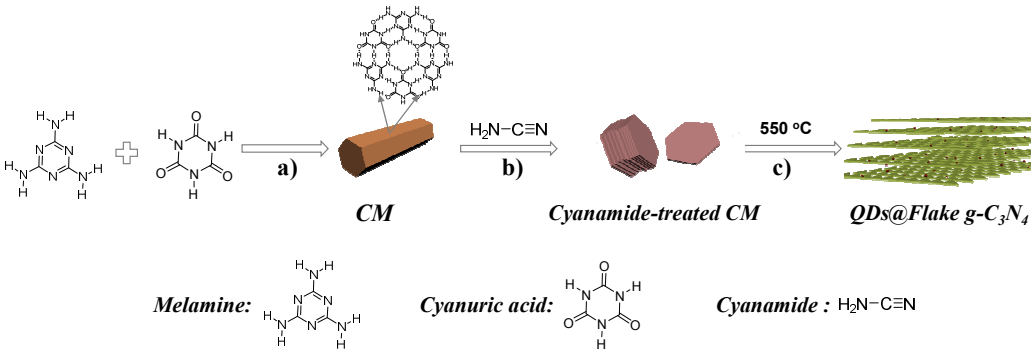

Scheme 1. Preparation procedure of QDs@Flake g-C_3N_4: a) the formation of hydrogen-bonded CM, b) the treatment of CM with cyanamide, and c) the thermal polycondensation of cyanamide-treated CM through calcination at 550 ^oC.

Scheme 1 shows the preparation procedure of QDs@Flake *g*-C_3N_4, which includes a) the formation of hydrogen-bonded CM, b) the treatment of CM with cyanamide, and c) the thermal polycondensation of cyanamide-treated CM through calcination. Specifically, the rapid precipitation of CM was implemented through mixing equal amount of cyanuric acid and melamine in deionized water. The resultant CM was crystallized into a rod-like hexagonal prism primarily based on hydrogen bonding between cyanuric acid and melamine (**Figure S1**a). [25, 27] After treated by cyanamide, CM showed morphological changes from rods to irregular lamellar-reduced stacking

structure (**Figure S1**b). The crystal structures of CM before and after cyanamide treatment were quite similar as indicated in the X-ray diffraction (XRD) patterns (**Figure S1**c). However, these two samples of CM and cyanamide-treated CM showed significant difference in crystal structure compared to sole cyanuric acid or melamine, where some new XRD peaks appeared at 10.52°, 21.32° and 27.82° (**Figure S1**c). These peaks indicated strong evidence of the crystal structure changes caused by the complexion of cyanuric acid and melamine. Then, the chemical composition of cyanuric acid, melamine, CM and cyanamide-treated CM was examined by using of Fourier transform infrared (FTIR) spectroscope (**Figure S1**d). Compared to cyanuric acid and melamine, CM and cyanamide-treated CM showed more complicated curves with several new absorption bands. [28] By contrast, CM and cyanamide-treated CM possessed much similar FTIR absorption bands, which further suggested the minor influence of adding cyanamide on the changes of chemical composition of CM.

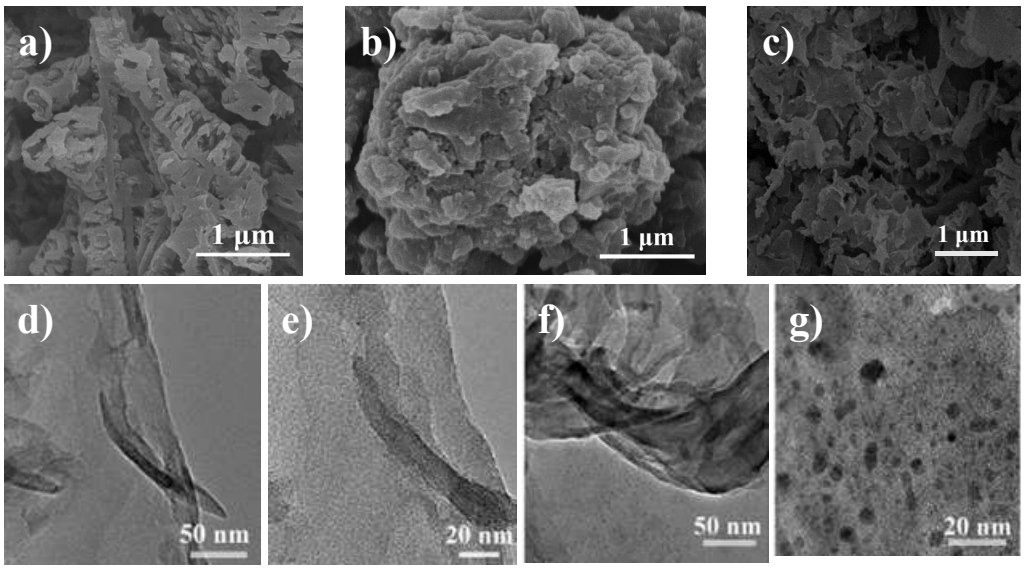

Figure 1 SEM images of a) g-C_3N_4-CM, b) g-C_3N_4-Cya and c) QDs@Flake g-C_3N_4.

High-resolution TEM images of d, e) g-C_3N_4-CM and f, g) QDs@Flake g-C_3N_4.

After the calcination of CM, cyanamide and cyanamide-treated CM, g-C_3N_4 with different morphologies were obtained and then characterized by scanning electron microscope (SEM, **Figure 1**a-c). In detail, g-C_3N_4 derived from CM showed tubular structures with a broken shell, which is in line with previous literature. [29] After treatment with cyanamide, the supramolecular CM was transformed into flake-shape g-C_3N_4 as evidenced by SEM and transmission electron microscopy (TEM) images (**Figure S2**a). The flake-shape g-C_3N_4 also exhibited a remarkable difference in morphologies compared to cyanamide-derived g-C_3N_4 (termed as g-C_3N_4-Cya, bulky in shape (Figure S3)). The surface microstructure of the flake-shape g-C_3N_4 was then examined by high-resolution TEM (**Figure 1**f, g), which showed numerous quantum dots (QDs, ~3 nm in average as shown in Figure S4) g-C_3N_4 dispersed on the flake (HRTEM, **Figure 1**d, e), indicating the formation of QDs@Flake g-C_3N_4. This unique two-dimensional (2D) flake structure rendered a relatively higher specific surface area for light harvesting, and 2D structures for the oriented transfer of charges. Meanwhile, the two moieties of g-C_3N_4, *i.e.*, QDs and flake, showed great potentials in generating isotype heterojunctions.

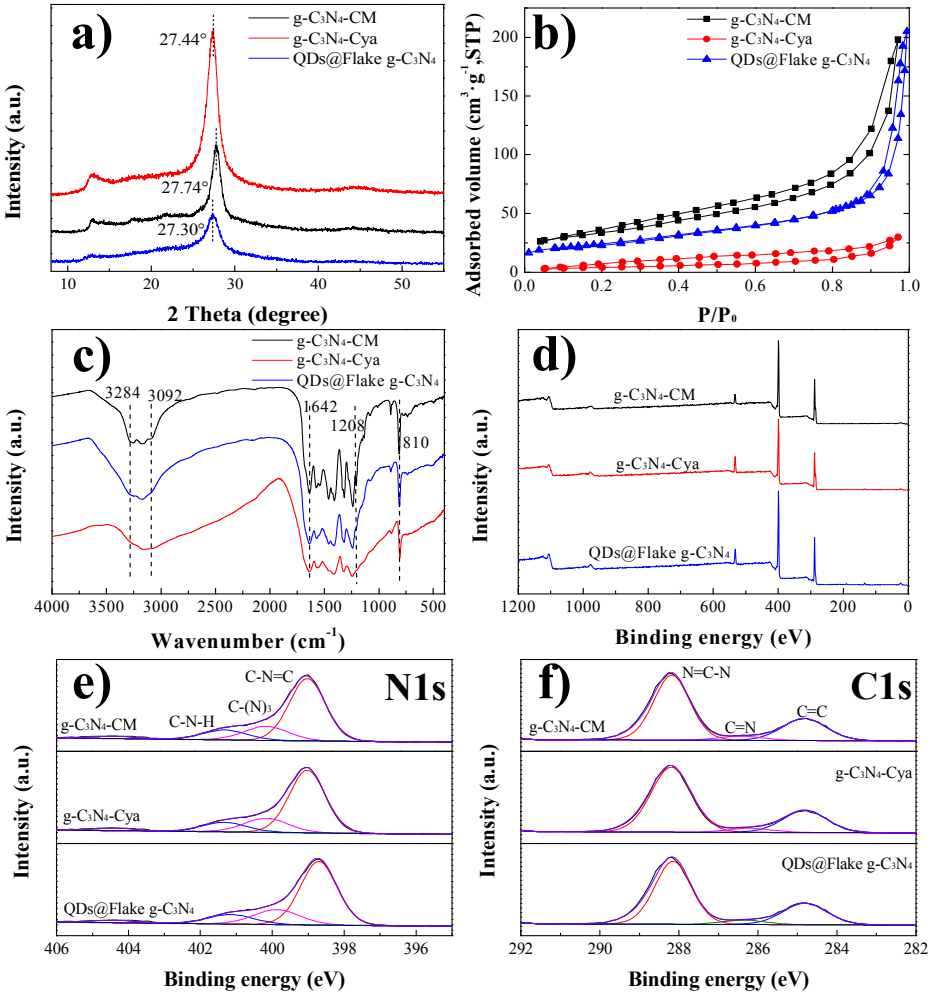

Figure 2 a) XRD patterns and b) N_2 adsorption isotherms of g-C_3N_4-CM, g-C_3N_4-Cya and QDs@Flake g-C_3N_4. c) FTIR spectra, d) X-ray photoelectron spectroscopy (XPS), and the corresponding e) N1s and f) C1s spectra of g-C_3N_4-CM, g-C_3N_4-Cya and QDs@Flake g-C_3N_4.

The textural and chemical structures of g-C_3N_4-CM, g-C_3N_4-Cya and QDs@Flake g-C_3N_4 were further characterized by XRD, nitrogen adsorption-desorption isotherms, FTIR and XPS (**Figure 2**). [30] The XRD patterns (**Figure 2**a) indicated that all three

g-C_3N_4 featured two peaks: the low-angle reflection peak at around 13^o stemmed from the interplanar structural packing, and the strong peak at around 27^o represented the characteristic stacking structure of g-C_3N_4 layers. [31] The interplanar crystal spacing of g-C_3N_4-CM and QDs@Flake g-C_3N_4 was calculated as 0.321 nm (27.74^o) [32] and 0.326 (27.30^o). This indicated that QDs slightly widened the interplanar crystal spacing between the neighbored layers of QDs@Flake g-C_3N_4. As shown in **Figure 2**b, both g-C_3N_4-CM and QDs@Flake g-C_3N_4 showed higher N_2 adsorption capacities all through the applied pressure when compared to g-C_3N_4-Cya. In detail, the surface areas of g-C_3N_4-CM and QDs@Flake g-C_3N_4 were, respectively, 113.2 m^2 g^{-1} and 84.92 m^2 g^{-1}, which were over 7 times higher than that of g-C_3N_4-Cya (12.72 m^2 g^{-1}) due to their tubular or flake structure. The FTIR absorption bands in **Figure 2**c indicated that QDs@Flake g-C_3N_4 had similar chemical compositions as g-C_3N_4-CM and g-C_3N_4-Cya. The bands between 3500 and 3100 cm^{-1} were assigned to the stretching vibration of -NH_2 or H_2O groups. The broad peaks between 1600 and 1200 cm^{-1} were ascribed to the stretching vibration of melon such as trigonal C-N=C or bridging C-NH-C unit. The sharp peak at ~810 cm^{-1} belonged to the breathing mode of tri-*s*-triazine rings. [30] Moreover, XPS results showed the similarity in surface elemental composition among g-C_3N_4-CM, g-C_3N_4-Cya and QDs@Flake g-C_3N_4 (**Figure 2**d). Weak O1s peaks were probably caused by the adsorbed H_2O on the sample surface, also proved by FTIR spectra and thermo gravimetric (TG) analysis (Figure S6). High-resolution N1s spectra implied the existence of sp^2-hybridized nitrogen (398.68 eV), tertiary nitrogen (N-$(C)_3$) (399.68 eV) and amino groups

(401.18 eV) in all three samples (**Figure 2**e). An additional peak with rather weak intensity at 404.38 eV was also observed, which was ascribed to the π-excitation. Additionally, **Figure 2**f showed the high-resolution C1s spectra, which could be split into three characteristic peaks: 288.0 eV for N-C=N, 286.1 eV for C-N and 284.4 eV for C=C bands (**Figure 2**f). [33] In general, all samples were only composed of two abundant elements: carbon and nitrogen, which well matched with the energy dispersive X-ray (EDX) spectrum and elemental mapping analysis (**Figure S5**). The C/N atomic ratio for QDs@Flake g-C_3N_4 was ~0.68, a bit lower than the theoretical value of 0.75, which might be due to the existence of uncondensed –NH_2 groups.

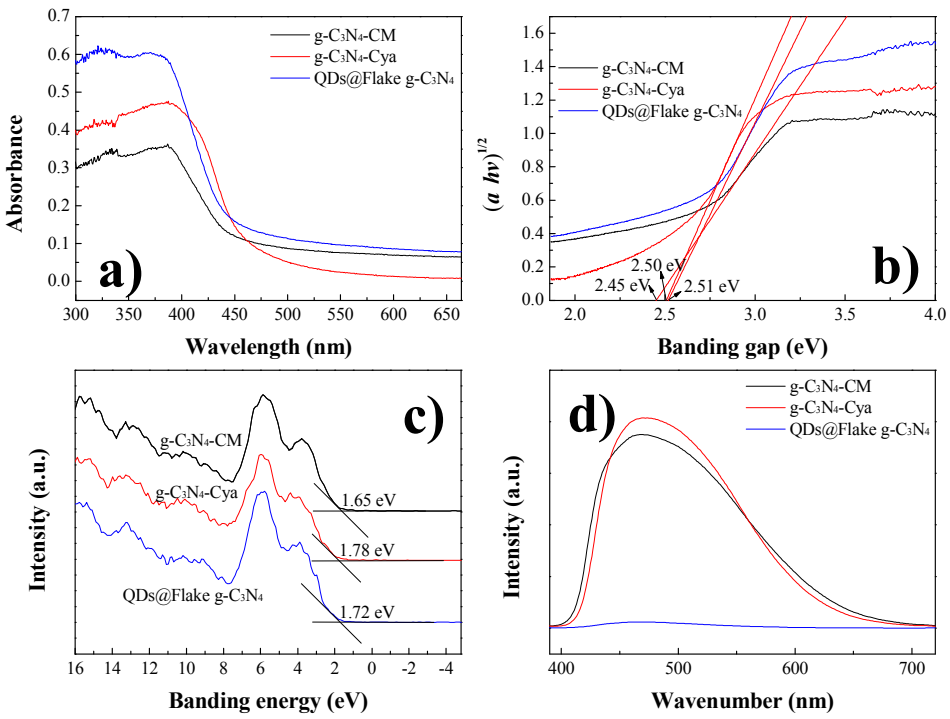

Figure 3 a) UV-Vis diffuse reflectance spectra, b) the corresponding plots of $(\alpha h\upsilon)^{1/2}$ versus photos energy, c) valence band XPS spectra, and d) PL spectra at the excitation wavelength of 375 nm of g-C_3N_4-CM, g-C_3N_4-Cya and QDs@Flak g-C_3N_4.

The electronic properties of g-C_3N_4 were commonly reflected in their photophysical property, which could be measured by the changes in the intensity or shape of UV-vis diffuse reflectance spectra. The UV-vis spectra suggested that the photo-absorption band edge of QDs@Flake g-C_3N_4 was situated between the photo-absorption band edge of g-C_3N_4-CM and g-C_3N_4-Cya. This phenomenon was mainly caused by the existence of two types of g-C_3N_4 (QDs and flake, **Figure 3**a). Moreover, the remarkably enhanced light-harvesting ability was observed for QDs@Flake g-C_3N_4 across the visible-light optical spectrum compared to g-C_3N_4-CM and g-C_3N_4-Cya. The shift arose from the variation of surface states was associated with their morphologies and band gap energy. As shown in **Figure 3**b and c, the band gap energy (E_g) estimated from the intercept of the tangents to the plots of $(\alpha h\upsilon)^{1/2}$ versus photon energy was 2.45, 2.50 and 2.51 eV for g-C_3N_4-CM, g-C_3N_4-Cya and QDs@Flake g-C_3N_4, respectively. Meanwhile, the valence band XPS spectra of the three samples were performed to determine the relative position of valence band edge of the samples, as presented in **Figure 3**c. Combined with the band gap energy obtained from UV-Vis diffuse reflectance spectra and the valence bands derived from XPS results, the conduction bands of g-C_3N_4-CM, g-C_3N_4-Cya and QDs@Flake g-C_3N_4 were, respectively, -0.80, -0.72 and -0.79 eV. The optical properties suggested that the textural structure of QDs@Flake g-C_3N_4 would be beneficial to improve visible-light harvesting ability, and have a positive influence on minimizing the recombination of photo-generated electrons-holes pairs. To verify this hypothesis, the

photoluminescence (PL) emission spectra of g-C_3N_4-CM, g-C_3N_4-Cya and QDs@Flake g-C_3N_4 were conducted and shown in **Figure 3**d. No apparent fluorescence emission peaks of QDs@Flake g-C_3N_4 were observed. By contrast, both of g-C_3N_4-CM and g-C_3N_4-Cya exhibited a much stronger peak, suggesting the superiority of 2D structured QDs@Flake isotype heterojuctions in facilitating the transfer and separation of photo-excited charge carriers.

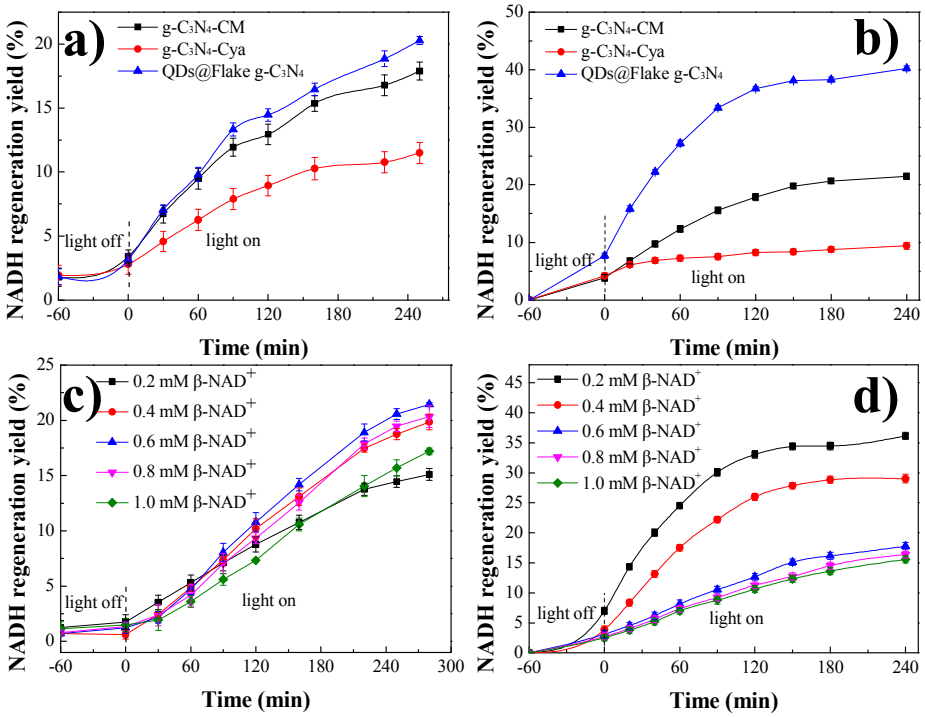

Figure 4 NADH regeneration yields enabled by g-C_3N_4-CM, g-C_3N_4-Cya and QDs@Flake g-C_3N_4 in the a) absence and b) presence of 0.25 mM mediator ($\lambda \geq 420$ nm, 0.1 M PBS pH = 9.0, TEOA 10.0 w/v%). NADH regeneration yields as a function of illumination time for QDs@Flake g-C_3N_4 with different β-NAD^+

concentrations in the c) absence and d) presence of 0.25 mM mediator ($\lambda \geq 420$ nm, 0.1 M PBS pH = 9.0, TEOA 10.0 w/v%, QDs@Flake g-C_3N_4 1.0 mg mL^{-1}).

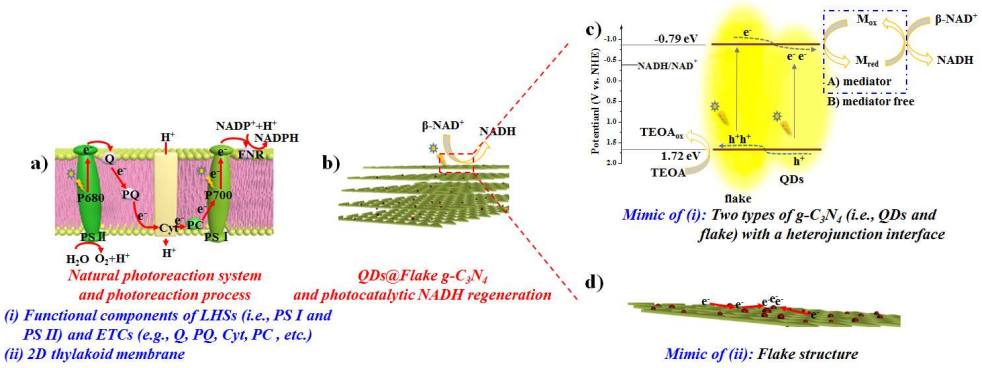

Scheme 2. a) Structural illustration of natural photoreaction system as well as the photoreaction process. b-d) Structural illustration of QDs@Flake g-C_3N_4 as well as the photocatalytic regeneration of NADH in the absence and presence of a mediator: c) QDs- and flake-moieties in QDs@Flake g-C_3N_4 are the mimics of PSI and PSII in LHSs, whereas the heterojunction interface is the mimic of ETCs; d) the 2D topological structure of QDs@Flake g-C_3N_4 is the mimic of 2D thylakoid membrane.

The photocatalytic performance of QDs@Flake g-C_3N_4, g-C_3N_4-CM and g-C_3N_4-Cya were demonstrated by the evolution of NADH under visible-light illumination at a wavelength $\lambda \geq 420$ nm in the absence and presence of a mediator ($[Cp^*Rh(bpy)(H_2O)]^{2+}$). [6, 26] Herein, it should be noted that, since the regeneration mechanism of NADH was quite different under the conditions of having a mediator or not. Therefore, we then would like to choose these two reaction modes to demonstrate

the superiority of QDs@Flake g-C_3N_4. In brief, in the absence of a mediator, β-NAD^+ would adsorb on the g-C_3N_4 through π–π stacking between the adenine subunit of β-NAD^+ and the tri-*s*-triazine units of g-C_3N_4. The π–π stacking results in the hydride transfer from g-C_3N_4 to β-NAD^+ and the subsequent NADH regeneration. [6, 26] In the presence of a mediator, photo-excited electrons could be firstly shuttled the mediator. The mediator is homogeneously dispersed in the solution and much easier to transfer electrons to β-NAD^+, facilitating the regeneration of NADH and commonly resulting in higher NADH regeneration yield compared to the reaction without a mediator. Accordingly, well matched the above-mentioned mechanisms and previous literatures, [6, 33]

an enhanced NADH regeneration yield was observed for g-C_3N_4 with a mediator rather than without a mediator (**Figure 4**a and b). More importantly, for both reaction modes, QDs@Flake g-C_3N_4 exhibited the highest NADH regeneration yield by contrast with g-C_3N_4-Cya and g-C_3N_4-CM during illumination as indicated in **Figure 4**a and b. Specifically, under certain conditions (*i.e.*, 0.6 mM β-NAD^+, no mediator, 4 h illumination) without a mediator, the NADH regeneration yield of QDs@Flake g-C_3N_4 could reach 22.5%, while g-C_3N_4-CM and g-C_3N_4-Cya only showed the NADH regeneration yields of 17.8% and 11.2%, respectively. With a mediator and under a shorter illustration time (2.5 h) with even a lower β-NAD^+ concentration (0.2 mM), QDs@Flake g-C_3N_4 could reach a much higher NADH regeneration yield of ~40.0% that was nearly two and five times higher than that of g-C_3N_4-CM and g-C_3N_4-Cya, respectively. Based on the above physiochemical characterizations and photocatalytic reaction, the enhancement of NADH regeneration yield upon

QDs@Flake g-C_3N_4 in each reaction mode should be ascribed to the following three aspects (**Scheme 2**), showing similarity to the natural photoreaction system: i) QDs- and flake-moieties in QDs@Flake g-C_3N_4 are the mimics of PSI and PSII in LHSs, respectively (**Scheme 2**a and c). The photo-generation of electron-hole pairs occurred in both QDs- and flake-moieties of QDs@Flake g-C_3N_4 through co-initiation under visible light, which could offer more amount of electrons around the conducting band of QDs-moiety than g-C_3N_4-Cya and g-C_3N_4-CM. ii) The heterojunction interface is the mimic of ETCs (**Scheme 2**a and c). Based on the heterojunction interface and band structure of QDs- and flake-moieties, the photo-generated electrons from the flake-moiety favor to transfer to the QDs-moiety, whereas the photo-generated holes from the QDs-moiety favor to transfer to the flake-moiety. Such kind of transfer behavior would result in an accumulation of electrons around the conducting band of QDs-moiety. iii) As the mimic of 2D thylakoid membrane, the 2D topological structure of QDs@Flake g-C_3N_4 (**Scheme 2**a and d) also contributes some to the accumulation of electrons in the conducting band of QDs-moiety as the photo-generated electrons in the flake-moiety favor to transfer along 2D direction, which was beneficial for rapid transfer of electrons to the QDs-moiety. [13, 34] The accumulated electrons caused by both aspects as mentioned above then supplied sufficient electrons to the mediator reduction, and finally led to the enhanced NADH regeneration compared to g-C_3N_4-Cya and g-C_3N_4-CM. [17]

The influence of β-NAD^+ concentration on the NADH regeneration yield of QDs@Flake g-C_3N_4 was further examined under successive illumination (**Figure 4**c

and d). No matter in what reaction mode (with or without a mediator), QDs@Flake g-C_3N_4 showed an illumination time-dominated photocatalytic activity. Longer illumination time commonly led to enhanced NADH regeneration yield because of accumulation of regenerated NADH in solution. However, for both reaction modes, much higher β-NAD^+ concentration resulted in the decrease of NADH regeneration yield. [6] Nonetheless, the average reaction rates for these two reaction modes showed an increasing trend, indicating higher β-NAD^+ concentration would be better for maintaining a higher reaction rate and better catalytic performance (**Figure S7**).

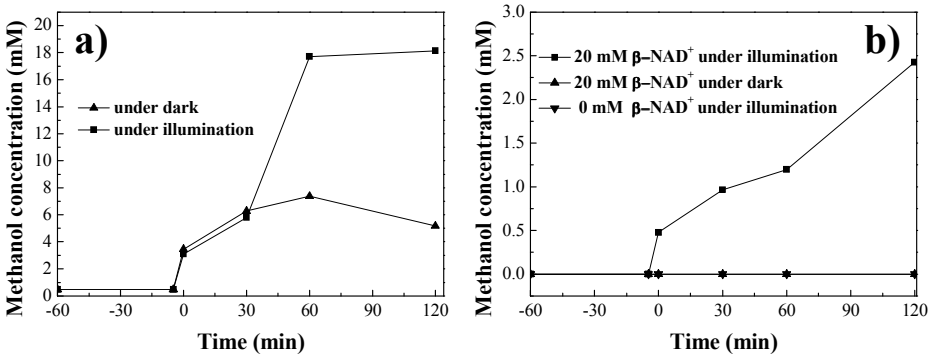

Figure 5 Photocatalytic NADH regeneration coupled with enzymatic hydrogenation of formaldehyde for methanol production. a) Temporal methanol concentration under illumination or dark over YADH (0.01 mg mL^{-1}) + NADH (20 mM) + QDs@Flake g-C_3N_4 (1.0 mg mL^{-1}). b) Temporal methanol yield over YADH (0.01 mg mL^{-1}) + mediator (0.25 mM) + QDs@Flake g-C_3N_4 (1.0 mg mL^{-1}) with β-NAD^+ (20 or 0 mM) under illumination or with β-NAD^+ (20 mM) under dark.

In situ regeneration of NADH is highly required for the sustainable synthesis of

chemicals and fuels through enzymatic hydrogenation. [35, 36] In this regards, photocatalytic regeneration of NADH was coupled with enzymatic hydrogenation of formaldehyde to methanol by yeast alcohol dehydrogenase (YADH) as shown in **Figure 5**. Methanol yield as a function of reaction time was assayed to examine the effectiveness of the regenerated NADH. In the absence of a mediator, the methanol yield was significantly influenced by the reaction conditions. More specifically, the reaction that carried out under illumination conditions exhibited a methanol yield of three times as high as that under dark conditions (**Figure 5**a), manifesting the feasibility of converting formaldehyde into methanol by coupling the regenerated NADH with YADH. However, with the prolongation of the reaction time for 60 min, the methanol yield was slightly reduced, which might be due to the partial volatilization of formaldehyde and methanol. Besides, β-NAD^+ as the initial substrate was then added to the coupled system to clarify the influence of NADH regeneration process on the catalytic performance of enzymatic hydrogenation. As shown in **Figure 5**b, methanol could not be generated either in the absence of β-NAD^+ or under dark. By contrast, the content of methanol increased progressively for the coupled system in the presence of β-NAD^+ under illumination. The methanol yield after reaction for 120 minutes was calculated to be ~8.3%, which is much better than our previous results using Pt/Al_2O_3 and H_2 for NADH regeneration (~2.7%). [7] It should be noted that 20 mM of NAD^+ used in **Figure 5** was higher than that of NAD^+ (0.2~1 mM) in **Figure 4**, which was to ensure a high concentration of methanol converted from formaldehyde for the accuracy of testing methanol content. More importantly,

the results again proved that the photocatalytic cofactor regeneration enabled by QDs@Flake g-C_3N_4 was successful, and also verified that the coupling of NADH regeneration with enzymatic hydrogenation was a feasible way to produce chemical and fuels.

4. CONCLUSIONS

In summary, QDs@Flake g-C_3N_4, a 2D isotype heterojunction photocatalyst, was prepared through one-step calcination of cyanamide-treated cyanuric acid-melamine complex for visible-light-driven NADH regeneration. The two types of g-C_3N_4, heterojunction interface and flake structure were, respectively, designed to mimic LHSs, ETCs and 2D thylakoid membrane in natural photoreaction system, conferring QDs@Flake g-C_3N_4 with enhanced visible-light harvesting ability and oriented transfer of electrons from flake to QDs. QDs@Flake g-C_3N_4 exhibited a much better performance in the photocatalytic regeneration of NADH either with or without a mediator in comparison to two other counterparts bearing no heterojunctions, *i.e.*, g-C_3N_4-CM and g-C_3N_4-Cya. The NADH regeneration system was then successfully coupled with enzymatic hydrogenation of formaldehyde for continuously producing methanol. This regeneration system could also be coupled with other NADH-dependent enzymatic hydrogenation processes.

ASSOCIATED CONTENT

Supporting information

SEM images of CM and cyanamide-treated CM; XRD patterns of melamine, cyanuric acid, CM and cyanamide-treated CM; FTIR spectra of melamine, cyanuric acid, CM, cyanamide-treated CM and cyanamide (Figure S1); TEM image of QDs@Flake g-C_3N_4; The pore size distribution of g-C_3N_4-CM, g-C_3N_4-Cya and QDs@Flake g-C_3N_4 (Figure S2); TEM image of g-C_3N_4-Cya (Figure S3); HRTEM image and size distributions histogram of QDs@Flake g-C_3N_4 (Figure S4); The EDX spectrum and elemental mapping analysis of QDs@Flake g-C_3N_4 (Figure S5); TG curves of g-C_3N_4-CM, g-C_3N_4-Cya and QDs@Flake g-C_3N_4 (Figure S6); and average reaction rates for NADH regeneration reactions as a function of NAD^+ concentration in the absence and presence of a mediator (Figure S7).

AUTHOR INFORMATION

Corresponding Author

E-mail: Jiafu Shi, shijiafu@tju.edu.cn; Zhongyi Jiang, zhyjiang@tju.edu.cn

ACKNOWLEDGEMENTS

The authors thank the financial support from National Natural Science Funds of China (21406163, 91534126, 21621004), Tianjin Research Program of Application Foundation and Advanced Technology (15JCQNJC10000), Open Funding Project of the National Key Laboratory of Biochemical Engineering (2015KF-03), and the Program of Introducing Talents of Discipline to Universities (B06006). X.W. also acknowledges financial support from The Carnegie Trust for the Universities of Scotland (70265) and The Royal Society (RG150001 and IE150611).

REFERENCES

(1) Shi, J.; Jiang,Y.; Jiang, Z.; Wang, X.; Zhang, S.; Han, P.; Yang, C. Enzymatic conversion of carbon dioxide. *Chem. Soc. Rev.* **2015**, *44*, 5981-6000.

(2) Dibenedetto, A.; Stufano, P.; Macyk, W.; Baran, T.; Fragale, C.; Costa, M.; Aresta, M. Hybrid technologies for an enhanced carbon recycling based on the enzymatic reduction of CO_2 to methanol in water: chemical and photochemical NADH regeneration. *ChemSusChem*, **2012**, *5*, 373-378.

(3) Wu, H.; Tian, C.; Song, X.; Liu, C.; Yang, D.; Jiang, Z. Methods for the regeneration of nicotinamide coenzymes. *Green Chem.* **2013**, *15*, 1773-1789.

(4) Geier, M.; Brandner, C.; Strohmeier, G. A.; Hall, M.; Hartner, F. S.; Glieder, A. Beilstein J. Org. Engineering Pichia pastoris for improved NADH regeneration: A novel chassis strain for whole-cell catalysis. *Chem.* **2015**, *11*, 1741-1748.

(5) Cazelles, R.; Liu, J.; Antonietti, M. Hybrid C_3N_4/fluorine-doped tin oxide electrode transfers hydride for 1, 4-NADH cofactor regeneration. *ChemElectroChem*, **2015**, *2*, 333-337.

(6) Huang, J.; Antonietti, M.; Liu, J. Bio-inspired carbon nitride mesoporous spheres for artificial photosynthesis: photocatalytic cofactor regeneration for sustainable enzymatic synthesis. *J. Mater. Chem. A*, **2014**, *2*, 7686-7693.

(7) Wang, X. Yiu, H. H. P. Heterogeneous catalysis mediated cofactor NADH regeneration for enzymatic reduction. *ACS Catal.* **2016**, *6*, 1880-1886.

(8) van Eerden, F. J.; van den Berg, T.; Frederix, P. W.; de Jong, D. H.; Periole X.; Marrink, S. J. Molecular dynamics of photosystem II embedded in the thylakoid

membrane. *J. Phys. Chem. B* **2016**, DOI: 10.1021/acs.jpcb.6b06865.

(9) Nozue, H.; Oono, K.; Ichikawa, Y.; Tanimura, S.; Shirai, K.; Sonoike, K.; Nozue, M.; Hayashida, N. Significance of structural variation in thylakoid membranes in maintaining functional photosystems during reproductive growth. *Physiol. Plant.* **2016**, DOI: 10.1111/ppl.12528.

(10) Azadi Chegeni, F.; Perin, G.; Sai Sankar Gupta, K. B.; Simionato, D.; Morosinotto, T.; Pandit, A. Protein and lipid dynamics in photosynthetic thylakoid membranes investigated by in-situ solid-state NMR. *Biochim. Biophys. Acta*, **2016**, *1857*, 1849-1859.

(11) Cardona, T.; Battchikova, N.; Zhang, P.; Stensjo, K.; Aro, E. M.; Lindblad, P.; Magnuson, A. Electron transfer protein complexes in the thylakoid membranes of heterocysts from the cyanobacterium Nostoc punctiforme. *Biochim. Biophys. Acta*, **2009**, *1787*, 252-263.

(12) Quinto, T.; Köhler V.; Ward, T. R. Recent trends in biomimetic NADH regeneration. *Top. Catal.* **2013**, *57*, 321-331.

(13) Ryu, J.; Lee, S. H.; Nam, D. H.; Park, C. B. Rational design and engineering of quantum-dot-sensitized TiO_2 nanotube arrays for artificial photosynthesis. *Adv. Mater.* **2011**, *23*, 1883-1888.

(14) Kim, J. H.; Lee, M.; Lee, J. S.; Park, C. B. Self-assembled light-harvesting peptide nanotubes for mimicking natural photosynthesis. *Angew. Chem. Int. Ed.* **2012**, *51*, 517-520.

(15) Yadav, R. K.; Oh, G. H.; Park, N. J.; Kumar, A.; Kong, K. J.; Baeg, J. O. Highly

selective solar-driven methanol from CO_2 by a photocatalyst/biocatalyst integrated system. *J. Am. Chem. Soc.* **2014**, *136*, 16728-16731.

(16) Oppelt, K. T.; Gasiorowski, J.; Egbe, D. A.; Kollender, J. P.; Himmelsbach, M.; Hassel, A. W.; Sariciftci, N. S.; Knor, G. Rhodium-coordinated poly(arylene-ethynylene)-alt-poly(arylene-vinylene) copolymer acting as photocatalyst for visible-light-powered NAD^+/NADH reduction. *J. Am. Chem. Soc.* **2014**, *136*, 12721-12729.

(17) Tong, Z.; Yang, D.; Sun, Y.; Nan, Y.; Jiang, Z. Tubular g-C_3N_4 isotype heterojunction: enhanced visible-light photocatalytic activity through cooperative manipulation of oriented electron and hole transfer. *Small* **2016**, *12*, 4093-4101.

(18) Dong, F.; Ni, Z.; Li, P.; Wu, Z. A general method for type I and type II g-C_3N_4/g-C_3N_4 metal-free isotype heterostructures with enhanced visible light photocatalysis. *New J. Chem.* **2015**, *39*, 4737-4744.

(19) Choudhury, B.; Giri, P. K. Isotype heterostructure of bulk and nanosheets of graphitic carbon nitride for efficient visible light photodegradation of methylene blue. *RSC Adv.* **2016**, *6*, 24976-24984.

(20) Zhang, J.; Zhang, M.; Sun, R. Q.; Wang, X. A facile band alignment of polymeric carbon nitride semiconductors to construct isotype heterojunctions. *Angew. Chem. Int. Ed.* **2012**, *51*, 10145-10149.

(21) Dang, X.; Zhang, X.; Zhang, W.; Dong, X.; Wang, G.; Ma, C.; Zhang, X.; Ma, H.; Xue, M. Ultra-thin C_3N_4 nanosheets for rapid charge transfer in the core–shell heterojunction of α-sulfur@C_3N_4 for superior metal-free photocatalysis under visible

light. *RSC Adv.* **2015**, *5*, 15052-15058.

(22) Ong, W. J.; Tan, L. L.; Ng, Y. H.; Yong, S. T.; Chai, S. P. Graphitic carbon nitride ($g\text{-}C_3N_4$)-based photocatalysts for artificial photosynthesis and environmental remediation: Are we a step closer to achieving sustainability? *Chem. Rev.* **2016**, *116*, 7159-7329.

(23) Tong, J.; Zhang, L.; Li, F.; Li, M.; Cao, S. An efficient top-down approach for the fabrication of large-aspect-ratio $g\text{-}C_3N_4$ nanosheets with enhanced photocatalytic activities. *Chem. Chem. Phys.* **2015**, *17*, 23532-23537.

(24) Zhang, X.; Xie, X.; Wang, H.; Zhang, J.; Pan, B.; Xie, Y. Processing pathway dependence of amorphous silica nanoparticle toxicity: colloidal vs pyrolytic. *J. Am. Chem. Soc.* **2013**, *135*, 18-21.

(25) Shalom, M.; Inal, S.; Fettkenhauer, C.; Neher, D.; Antonietti, M. Improving carbon nitride photocatalysis by supramolecular preorganization of monomers. *J. Am. Chem. Soc.* **2013**, *135*, 7118-7121.

(26) Liu, J.; Antonietti, M. Bio-inspired NADH regeneration by carbon nitride photocatalysis using diatom templates. *Energy Environ. Sci.* **2013**, *6*, 1486-1493.

(27) Dante, R. C.; Sánchez-Arévalo, F. M.; Chamorro-Posada, P.; Vázquez-Cabo, J.; Huerta, L.; Lartundo-Rojas, L.; Santoyo-Salazar, J.; Solorza-Feria, O. Supramolecular intermediates in the synthesis of polymeric carbon nitride from melamine cyanurate. *J. Solid State Chem.* **2015**, *226*, 170-178.

(28) Arrachart, G.; Carcel, C.; Trens, P.; Moreau, J. J.; Wong Chi Man, M. Silylated melamine and cyanuric acid as precursors for imprinted and hybrid silica materials

with molecular recognition properties. *Chem.* **2009**, *15*, 6279-6288.

(29) Guo, S.; Deng, Z.; Li, M.; Jiang, B.; Tian, C.; Pan, Q.; Fu, H. Phosphorus-doped carbon nitride tubes with a layered micro-nanostructure for enhanced visible-light photocatalytic hydrogen evolution. *Angew. Chem. Int. Ed.* **2016**, *55*, 1830-1834.

(30) Liang, Q.; Li, Z.; Yu, X.; Huang, Z. H.; Kang, F.; Yang, Q. H. Macroscopic 3D porous graphitic carbon nitride monolith for enhanced photocatalytic hydrogen evolution. *Adv. Mater.* **2015**, *31*, 4634-4639.

(31) Kang, Y.; Yang, Y.; Yin, L. C.; Kang, X.; Liu, G.; Cheng, H. M. An amorphous carbon nitride photocatalyst with greatly extended visible-light-responsive range for photocatalytic hydrogen generation. *Adv. Mater.* **2015**, *27*, 4572-4577.

(32) Han, Q.; Wang, B.; Zhao, Y.; Hu, C.; Qu, L. A Graphitic-C_3N_4 "seaweed" architecture for enhanced hydrogen evolution. *Angew. Chem. Int. Ed.* **2015**, *39*, 11433-11437.

(33) Li, H. J.; Sun, B. W.; Sui, L.; Qian, D. J.; Chen, M. Preparation of water-dispersible porous g-C_3N_4 with improved photocatalytic activity by chemical oxidation. *Phys. Chem. Chem. Phys.* **2015**, *17*, 3309-3315.

(34) Zhang, J.; Chen, X.; Takanabe, K.; Maeda, K.; Domen, K.; Epping, J. D.; Fu, X.; Antonietti, M.; Wang, X. Synthesis of a carbon nitride structure for visible-light catalysis by copolymerization. *Angew. Chem. Int. Ed.* **2010**, *49*, 441-444.

(35) Ji, X.; Su, Z.; Wang, P.; Ma, G.; Zhang, S. Tethering of nicotinamide adenine dinucleotide inside hollow nanofibers for high-yield synthesis of methanol from carbon dioxide catalyzed by coencapsulated multienzymes. *ACS Nano*, 2**015**, *9*,

4600-4610.

(36) Denard, C. A.; Hartwig, J. F.; Zhao, H. Multistep one-pot reactions combining biocatalysts and chemical catalysts for asymmetric synthesis. *ACS Catal.* **2013**, *3*, 2856-2864.

Table of Contents